CrossMark

ORIGINAL PAPER

Fe@Pt core-shell nanoparticles as electrocatalyst for oxygen reduction reaction in acidic media

Yanli Huang[1] · Zhan Tan[1] · Huimin Wu[1] · Chuanqi Feng[1] · Yu Ding[2]

Abstract To settle the drawbacks of non-cost-effective and enhance the electrocatalytic performance of Pt/C, Fe@Pt core-shell nanoparticles supported by Vulcan XC-72 have been designed and synthetized successfully. The synthesized materials were characterized by X-ray diffraction, scanning electron microscopy, transmission electron microscopy, and X-ray photoelectron spectroscopy, whereas the electrochemical analyses were obtained by electrochemical impedance spectroscopy, cyclic voltammetry, linear sweep voltammetry, and chronoamperometry. Results suggest that the onset potential of oxygen reduction reaction on the Fe@Pt/C is about 0.6 V (vs. Hg/Hg_2Cl_2) in O_2-saturated 0.5 M H_2SO_4, which shifts positively more than 30 mV compared with that of Pt/C. The corresponding electron transfer number is 4, meaning the reduction reaction mainly occurred through a 4-electron pathway. More importantly, the Fe@Pt/C has an excellent stability and better catalytic performance towards oxygen reduction reaction activity compared with Pt/C. Thus, Fe@Pt/C could be utilized as promising cathode catalysts in proton exchange membrane fuel cells.

Introduction

Proton exchange membrane fuel cells (PEMFC) based on oxygen reduction reaction (ORR) at the cathode [1] have emerged as very promising energy conversion devices for automotive, portable or stationary systems, because of their low working temperature, high efficiency, and environment friendliness [2–7]. Unfortunately, the sluggish reaction kinetics of ORR would hinder further developments of PEMFC [8, 9]. To settle this issue, high efficient electrocatalyst towards ORR is required. According to previous reports, platinum (Pt) is the predominant choice for its function in promoting the electron transfer and reducing the overpotential [10]. However, the high costs resulting from the excessive usage of Pt and the scarcity of Pt are still considered as critical hurdles for the prevalent commercialization of the PEMFC technology [11–14].

To enhance the electrocatalytic performance and reduce the usage of Pt, alloying Pt with less expensive transition metals (such as Fe, Co, Ni, and Cu) has been actively studied [11–16]. The enhancement electrocatalytic activity results from the effect that alloying Pt with less expensive transition metals can favorably tune the electronic structure of Pt and leads to a down shift of the Pt d-band center [17–19]. However, the unstability of the Pt-based alloy resulting from the dissolution of transition metals is another problem. To enhance the stability of the Pt-based alloy, Pt-based bimetallic core-shell structured electrocatalysts have obtained considerable attentions. Previous reports have proved that the core-shell architecture of Pt-based materials exhibits superior catalytic properties and stability. At the same time, previous

✉ Huimin Wu
whm267@126.com

✉ Yu Ding
sunny_boy168@sina.com

[1] Hubei Collaborative Innovation Center for Advanced Organic Chemical Materials & Key Laboratory for the Synthesis and Application of Organic Functional Molecules, Ministry of Education & College of Chemistry & Chemical Engineering, Hubei University, Wuhan 430062, People's Republic of China

[2] College of Chemistry and Materials Science, Hubei Engineering University, Xiaogan 432000, China

reports showed that the iron (Fe) is widely used as a catalyst in the field of growth of carbon nanotubes and [20] ammonia decomposition [21]. We have already studied the Fe@Pt application in detection of hydrogen peroxide, glucose, and formaldehyde [22].

Herein, Fe@Pt core-shell nanoparticles are prepared and can be used as advanced electrocatalysts towards ORR in acidic media. The results show that the Fe@Pt/C exhibits better electrocatalytic activity and stability towards ORR than Pt/C.

Experimental

Preparation of Fe@Pt/C

Without other mentioned, all reagents involved were analytical grade and available from Sinopharm Chemical Reagent Co. Ltd. And deionized water was used through the whole process.

The Fe@Pt nanoparticles were prepared similar to previous reports [23, 24]. Briefly, $Fe(NO_3)_3 \cdot 9H_2O$ was reduced by ascorbic acid under vigorous stirring for 1 h. After that, K_2PtCl_4 solution (pH 2.5) was added dropwise into the above solution. Then, the black suspension was isolated and washed. The Fe@Pt nanoparticles were dispersed on carbon particles (Vulcan XC-72) to obtain Fe@Pt/C. Procedure details have been reported elsewhere [22].

Physical characterization

The physical phases of electrocatalysts were studied by X-ray diffraction (XRD) (Bruker D8 Advance). Field emission gun scanning electron microscopy (FEG-SEM) (JEOL 7001F) equipped with energy dispersive X-ray spectroscopy was used to get the morphology image and semi-quantitative information. The size and distribution of the electrocatalyst were evaluated by means of transmission electron microscopy (TEM) (JEOL JEM 2011). The binding energy was studied by X-ray photoelectron spectroscopy (XPS) (ESCALAB 250Xi) equipped with the monochromatic Al K_α source.

Electrochemical tests

The electrochemical tests were performed using CHI 750E Electrochemical Workstation (CH Instrument Company, Shanghai, China), while the rotating disk electrode (RDE, Φ = 5 mm, Pine Instrument Company, USA) served as the working electrode. The counter electrode was Pt foil, and the reference electrode was a saturated calomel electrode (SCE); so all potentials are reported with respect to the SCE throughout this paper. The Fe@Pt/C (5 mg) was dispersed in 2-propanol (0.5 mL) by ultrasonic agitation for 60 min to form

homogeneous suspension and then, 12 μL (0.12 mg catalyst) of the suspension was dropped onto the polished RDE. After that, 3 μL Nafion (5%) was dropped onto the surface of the RDE. For comparison, the commercial Pt/C (BASF), glassy carbon electrode (GCE), and XC-72 carbon-modified GCE (C/GCE) were also tested at the same condition.

Results and discussion

Characterization of the Fe@Pt/C

The XRD was carried out to study the physical phase of the nanoparticles, and the results are shown in Fig. 1a. Obviously, there are three diffraction peaks for both nanoparticles. And all peaks are confirmed with the Pt phase (No. 011194). No characteristic diffraction peaks of Fe are observed, suggesting hardly any Fe atom on the surface of Pt in the Fe@Pt nanoparticles. What is more, these three diffraction peaks of the Fe@Pt nanoparticles are shifted to higher 2θ, indicating the contraction of the lattice due to the presence of the Fe core and the lattice constant is smaller than that of Pt. Such behavior of core-shell-nanostructured catalysts has been reported previously in the literature [24–26]. The absence of any diffraction peaks of Fe is most likely due to the heavy atom effect from Pt as a result of the formation of Fe@Pt nanoparticles [27].

Figure 1b shows the FEG-SEM of the Fe@Pt nanoparticles. In general, they look like a hornet's nest and exhibit a fluffy cotton-like microstructure. The chemical composition of the obtained nanoparticles was determined using EDX analysis. The results indicated the presence of both Fe and Pt, with an atomic ratio of 33:67. The TEM image of Fe@Pt is shown in Fig. 1c, presenting that Fe@Pt disperses uniformly and has an average size of about 5 nm. The inset is the associated SAED, which is consistent with that of XRD.

The XPS spectra of the Fe@Pt nanoparticles before and after the Ar etching were used to further probe the core-shell structure of the particles. Before the Ar etching, the XPS spectra of Pt 4f in Pt nanoparticles (I) and Fe@Pt nanoparticles (II) are shown in Fig. 1d. By contrast, the bulk Pt (71.3 eV), the binding energy of Pt $4f_{7/2}$ in the Fe@Pt nanoparticles, shifts to 70.7 eV. This suggests that the Pt-shell's electronic structure is modified by the inner Fe core [28]. Figure 1e shows the XPS spectra of Fe 2p in the Fe@Pt nanoparticles after Ar etching. The peaks located at 706.8 and 720.3 eV can be associated with the peaks of Fe $2p_{3/2}$ and Fe $2p_{1/2}$, respectively, indicating the presence of zero-valent Fe in the sample. Meanwhile, the results show that the Fe/Pt molar ratio is zero before Ar etching and the Fe/Pt ratio increases with the increase of the etching time, which indicates that more Pt atoms were etched than Fe atoms. This result is in accordance with a core-shell structure including a core mainly made of Fe and a shell

Fig. 1 **a** XRD patterns of the prepared Pt nanoparticles (I) and Fe@Pt nanoparticles (II). **b** FEG-SEM image of Fe@Pt nanoparticles. **c** TEM image of Fe@Pt nanoparticles. *Inset* indicates selected area electron diffraction of Fe@Pt nanoparticles. **d** XPS spectra of Pt 4f in Pt nanoparticles (I) and Fe@Pt nanoparticles (II). **e** XPS spectra of Fe 2p in Fe@Pt nanoparticles
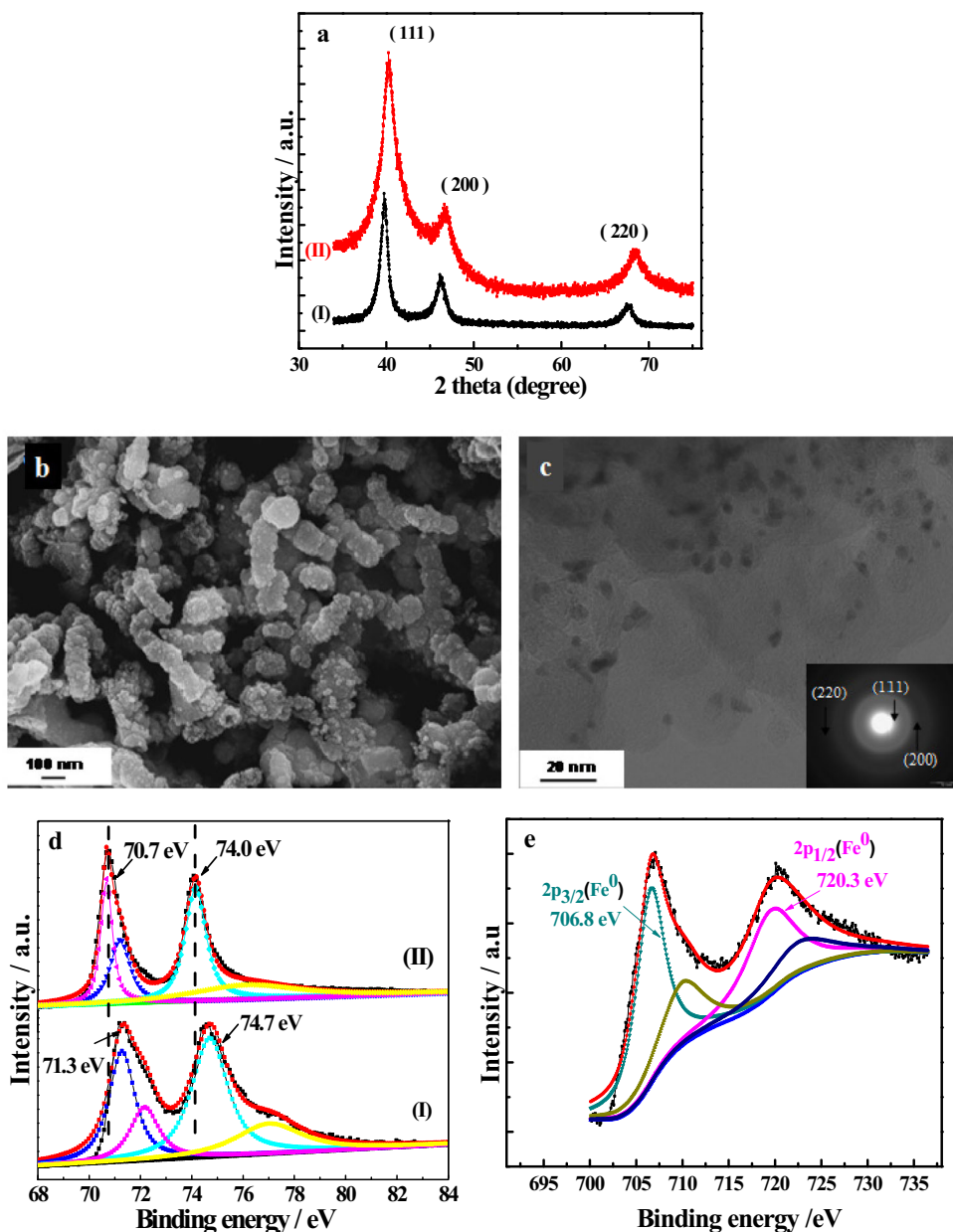
mainly made of Pt. The atomic ratio of Pt:Fe was determined to be 33:67, which is very close to the nominal ratio of 1:2.

Electrochemical performance of the Fe@Pt/C towards ORR

Figure 2a shows the electrochemical impedance spectroscopy (EIS) of the different modified electrodes in the given experiment condition (0.5 M H_2SO_4, 0.1 ~ 10^5 Hz). The semicircular part shows the electron transfer-limited process, the electron transfer resistance (R_{et}) is closely related with the diameter of the semicircular part at higher frequency. A smaller diameter of the arc indicates a lower R_{et} towards the ORR. For the Pt/C, the R_{et} is about 8.17 Ω, while the R_{et} of the

Fe@Pt/C is about 1.85 Ω. Therefore, the Fe@Pt/C shows better electron-conductivity properties than the Pt/C, and could afford much faster ORR kinetics.

Figure 2b shows cyclic voltammograms (CVs) of GCE (a), C/GCE (b), Pt/C (c), and Fe@Pt/C (d) in 0.5 M H_2SO_4. Both Fe@Pt/C and Pt/C exhibit the signatures of polycrystalline Pt in the given potential range (−0.20 ~ 0.90 V), which can be divided into the hydrogen adsorption/desorption peaks, a double layer region, and Pt oxide formation/stripping peaks [29]. A common belief is that the PtM alloys will not present these characteristic hydrogen peaks until the Pt contains more than 50.0 atom% [1, 30]. While the Fe@Pt nanoparticles contained less than 50.0 atom% (33.0 atom%) Pt, which indicates that it is the core-shell structure rather than the alloy structure. More
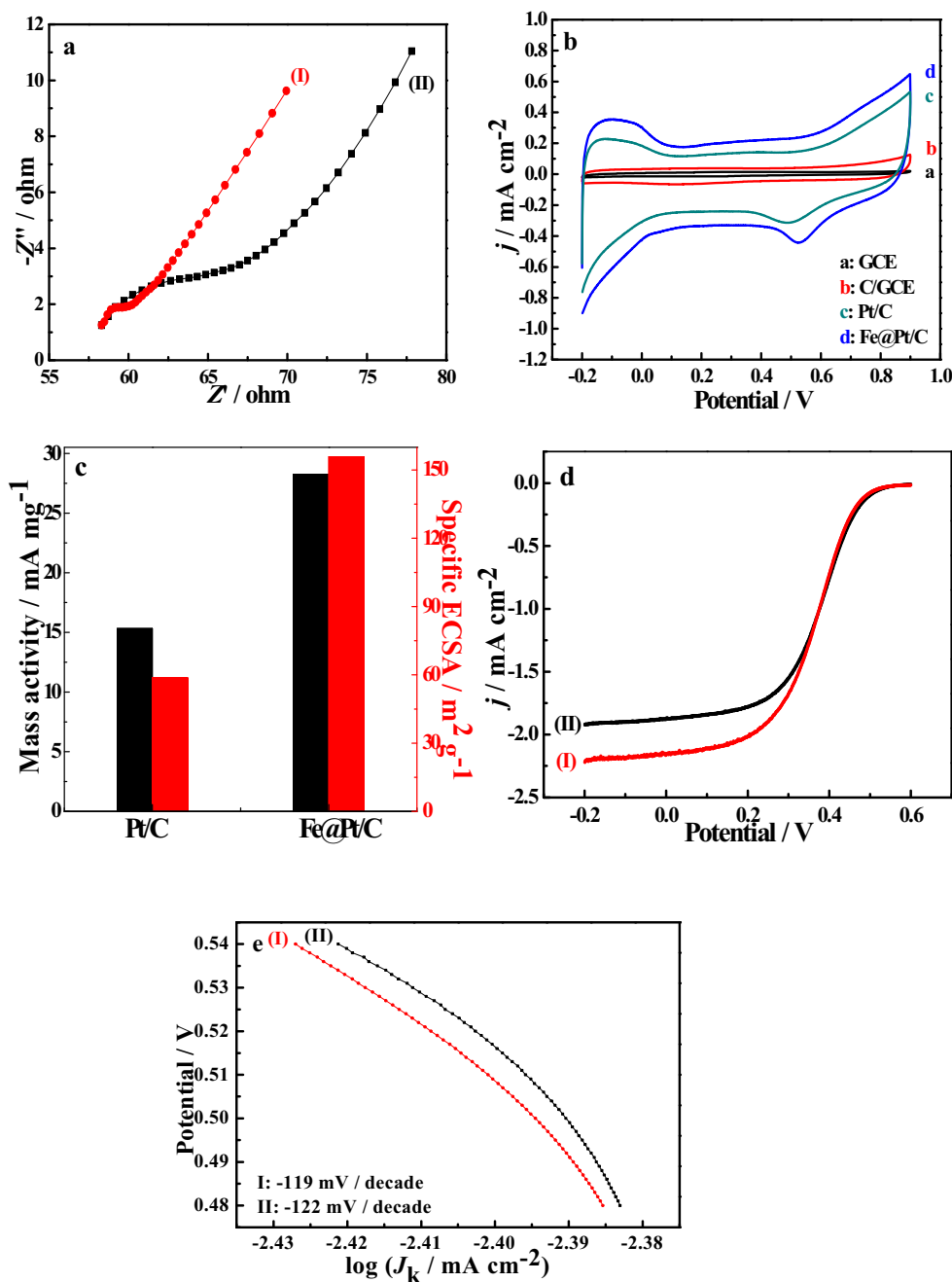
importantly, the absence of any characteristic peaks for Fe
dissolution in CVs showed that there is hardly any Fe atom
on the surface of Pt in the Fe@Pt nanoparticles and this also
may improve the stability of the catalyst in an acidic medium.
Actually, the different adsorption properties of supported met-
al monolayers from their parent metals have been shown to be
a general phenomenon due to the modification of electronic
properties of surface atoms by the underneath metal via geo-
metric strain and ligand interactions.

So we can deduce the core-shell structure from the follow-
ing analysis: (1) The results from XRD showed that the

nanoparticles were not physical mixtures of Fe and Pt, be-
cause they only had diffraction peaks of Pt; (2) CVs showed
Pt nature of the particle surface. Usually, the CVs obtained on
PtM alloys containing less than 50 atom% Pt do not exhibit
these hydrogen peaks, but the nanoparticles contained only
33.0 atom% Pt, which excluded the alloy structure; and (3)
The result from XPS demonstrated a core (Fe)-shell (Pt)
structure.

The catalytic performance of Pt-based hybrids can be
compared simply through the electrochemically active
surface area (ECSA), which can be calculated via the

Fig. 3 **a** LSVs of Fe@Pt/C catalysts in 0.5 M H_2SO_4 saturated with pure O_2 at a scan rate of 1 mV/s and at various rotation speeds (400, 625, 900, 1225, 1600, 2025, 2500 rpm). **b** Koutecky-Levich plots for the Fe@Pt/C catalysts at different voltages. **c** LSVs of Pt/C catalysts in 0.5 M H_2SO_4 saturated with pure O_2 at a scan rate of 1 mV/s and at various rotation speeds (400, 625, 900, 1225, 1600, 2025, 2500 rpm). **d** Koutecky-Levich plots for the Pt/C catalysts at different voltages
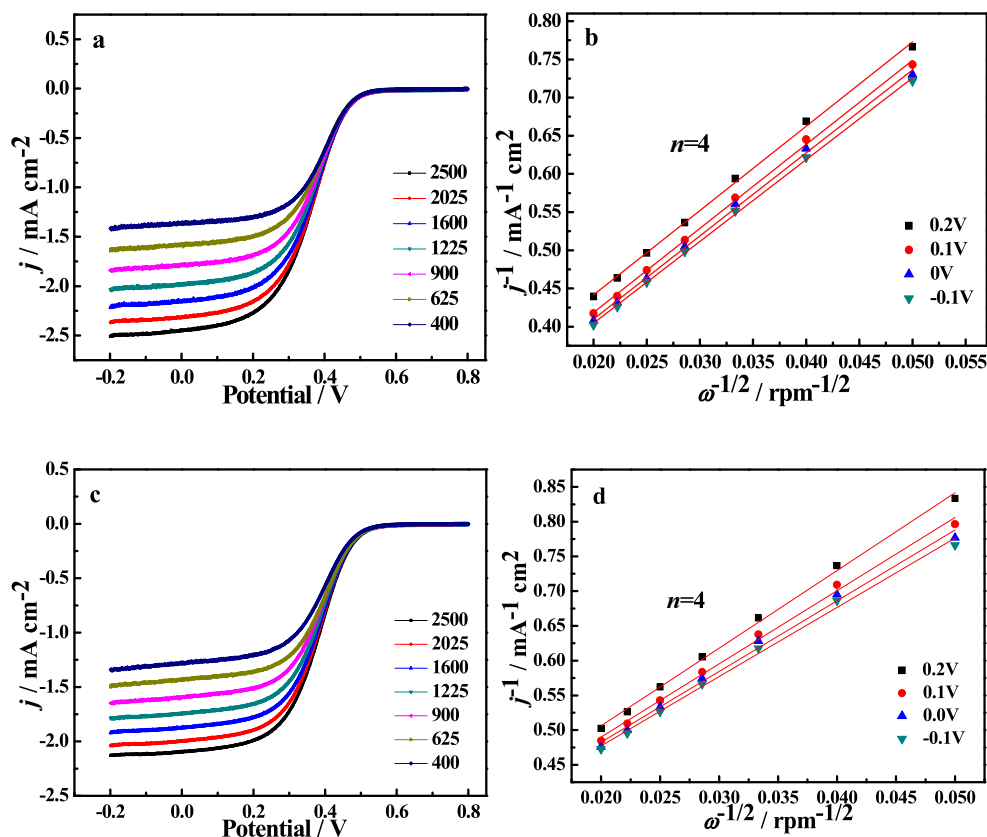
integral of hydrogen adsorption/desorption peaks using the following equation:

$$ECSA = Q_H/210 \,[Pt]$$

where Q_H (mC cm^{-2}) is the charge for hydrogen desorption without including the "double layer" region, [Pt] represents the loading of Pt on the electrode, and 210 μC cm^{-2} is the charge required to oxidize a monolayer of H_2 on the Pt site [31]. According to the CVs of the GCE and C/GCE in 0.5 M H_2SO_4 (Fig. 2b), the current in the "double layer" region is too low to be negligible. So as shown in Fig. 2c, the specific ECSA of Fe@Pt/C is 156 m^2 g^{-1}, while that of Pt/C is 58.1 m^2 g^{-1}. It indicates that

Table 1 The meanings, values, and units of involved letters

Letter	Meaning	Value and unit
J	Measured current density	mA cm^{-2}
J_K	Kinetic current density	mA cm^{-2}
J_L	Diffusion-limiting current density	mA cm^{-2}
ω	Rotation rate	rpm
F	Faraday constant	96,485 C mol^{-1}
C_0	Bulk concentration of O_2	1.1×10^{-6} mol cm^{-3}
D	Diffusion coefficient of O_2 in 0.5 M H_2SO_4	1.4×10^{-5} cm s^{-1}
ν	Viscosity of the electrolyte	0.01 cm^2 s^{-1}

Fe@Pt/C nanoparticles have more catalytic sites than those of Pt/C. In addition, the reduction potential of Pt oxide on the Fe@Pt/C shifts positively more than 30 mV compared with that of Pt/C. This suggests that the Pt oxide formation and stripping process on the cover of Fe@Pt/C nanoparticles may happen in an easier and faster way as a result of lower adsorption energy [13]. Obviously, the reduction currents at about 0.5 V (0.75 V vs. RHE) were dramatically increased in O_2-saturated 0.5 M H_2SO_4. For fuel cell anode, 0.75 V is a completely senseless potential, but it is very close to the potential of ORR cathode. Furthermore, the current density of the reduction peak of Fe@Pt/C is 1.8 mA cm^{-2}, which is bigger than that of Pt/C (1.2 mA cm^{-2}). Meanwhile, the mass activity of Fe@Pt/C (28.25 mA mg^{-1}) is better than that of Pt/C (15.34 mA mg^{-1}), and the mass activity is also listed in Fig. 2c. All the results suggest that the Fe@Pt/C has superior electrocatalytic activity than Pt/C.

The ORR activities of Fe@Pt/C and Pt/C were further evaluated by linear sweep voltammetry (LSV), and are presented in Fig. 2d. The onset potential is defined as the potential at which the current density is equal to zero. The more positive the onset potential is, the better electrocatalytic activity towards ORR they show [32]. Both curves have sharp slopes and quickly reach a terrace. Meanwhile, the onset potential (0.6 V vs. Hg/Hg$_2$Cl$_2$) and the diffusion-limited current density of Fe@Pt/C are bigger than those of Pt/C, which agrees with the result from CVs. Furthermore, Tafel plots of Fe@Pt/C and Pt/C derived from the

Fig. 4 **a** Chronoamperometric response of Fe@Pt/C (*I*) and Pt/C (*II*) catalysts in O$_2$-saturated 0.5 M H$_2$SO$_4$ at 0.5 V. **b** LSVs of Fe@Pt/C (*I*, *I'*) and Pt/C (*II*, *II'*) catalysts in O$_2$-saturated 0.5 M H$_2$SO$_4$ before (*I*, *II*) and after (*I'*, *II'*) the chronoamperometric test. **c** SEM image of Fe@Pt/C before (*c-1*) and after (*c-2*) the chronoamperometric test. **d** XRD of Fe@Pt/C before (*I*) and after (*II*) the chronoamperometric test. **e** XPS of Fe@Pt/C before (*I*) and after (*II*) the chronoamperometric test

corresponding LSV at 1600 rpm were shown in Fig. 2e. The linear part of the Tafel plots is fitted to the Tafel equation ($\eta = b\log j + \alpha$, where *j* is the current density, *b* is the Tafel slope, α is the transfer coefficient), and it is calculated that Tafel slopes

are 119 mV/decade (Fe@Pt/C) and 122 mV/decade (Pt/C), respectively. The lesser the Tafel slope is, the smaller the overpotential is at the same condition, proving a better electrocatalytic performance.

The polarization curves of the ORR on the Fe@Pt/C at different rotating rates are shown in Fig. 3a. The diffusion-limited current density increases when the rotating rates range from 400 to 2500 rpm owing to the shortened diffusion distance at high speeds. The mechanism was additionally examined with the Koutecky-Levich correlations by using formulas (1)–(3) [4], as follows:

$$\frac{1}{J} = \frac{1}{J_L} + \frac{1}{J_K} = \frac{1}{B\omega^{1/2}} + \frac{1}{J_K} \tag{1}$$

$$B = 0.2nFC_0D^{2/3}\nu^{-1/6} \tag{2}$$

$$J_K = nFkC_0 \tag{3}$$

The meanings, values, and units of the involved letters are presented in Table 1. The adopted constant 0.2 is showed in formula (2) when the rotating speed is conveyed by revolutions per minute. With the help of formulas (1) and (2), the n can be precisely calculated. As presented in Fig. 3b, the Koutecky-Levich plots present linear relationships between j^{-1} and $\omega^{-1/2}$ with a similar slope, suggesting first-order reaction kinetics with respect to the concentration of dissolved oxygen and a similar n value for ORR at different potentials [33]. As we have known, the ORR in an acidic solution occurring either via four-electron reduction processes where O_2 is directly reduced to H_2O or a two-electron reduction pathway involving the formation of H_2O_2 as an intermediate [34–36]. Generally, the four-electron reduction pathway is preferred, because it provides a faster oxygen reduction rate [37, 38]. The electron transfer number ($n \approx 4$) was calculated from the slopes of Koutecky-Levich plots, suggesting a four-electron transfer pathway of oxygen reduction on Fe@Pt/C. For comparison, the polarization curves of the ORR on the Pt/C at different rotation rates were also conducted (Fig. 3c), and similar to the Fe@Pt/C, the current density increased with increasing rotation rate owing to the shortened diffusion distance at high speeds. It also revealed a four-electron transfer at 0.2 to −0.1 V (Fig. 3d).

The stability is another important parameter for the practical application. To investigate the stability of Fe@Pt/C towards ORR, chronoamperometry was carried out at setting parameters (0.5 V, 0.5 M H_2SO_4, O_2-saturated, 20,000 s). We select the current at 1000 s as the standard and choose points after a constant duration. It also remains about 80% of the initial current for Fe@Pt/C, while the Pt/C almost only remains 5% (Fig. 4a). It indicates that the Fe@Pt/C has an excellent stability and better catalytic performance towards ORR activity compared with Pt/C. Meanwhile, the stability was also proved by LSV (0.5 M H_2SO_4, O_2-saturated). Obviously, the Fe@Pt/C exhibits superior

stability than Pt/C, with little decay in limited current density over 20,000 s of continuous test (Fig. 4b). To further verify the stability of the catalyst, the morphology and chemical composition of the catalyst retrieved after the chronoamperometric test are shown in Fig. 4c–d. The Fe@Pt/C sample after the chronoamperometric test has an interconnected particle-like morphology from its original like a hornet's nest, and no obvious difference. Furthermore, XRD analysis shows similar diffraction patterns. Remarkably, after the chronoamperometric test, XPS studies revealed no obvious chemical state change of Fe (Fig. 4e), suggesting an excellent stability of the Fe@Pt/C catalyst.

Conclusions

The Fe@Pt nanoparticles were synthesized successfully and the core-shell structure was verified by physical characterization. When utilized as electrocatalysts towards ORR in acidic media, the electrochemical results illuminate that the Fe@Pt nanoparticles exhibit high electrocatalytic activity through a four-electron transfer process with an excellent stability.

References

1. Santos LGRA, Oliveira CHF, Moraes IR, Ticianelli EA (2006) Oxygen reduction reaction in acid medium on Pt-Ni/C prepared by a microemulsion method. J Electroanal Chem 596:141–148

2. Yin SB, Cai M, Wang CQ, Shen PK (2011) Tungsten carbide promoted Pd-Fe as alcohol-tolerant electrocatalysts for oxygen reduction reactions. Energy Environ Sci 4:558–563

3. Zhao X, Yin M, Ma L, Ling L, Liu CP, Liao J-H, Lu TH, Xing W (2011) Recent advances in catalysts for direct methanol fuel cells. Energy Environ Sci 4:2736–2753

4. Wang Y, Song Q, Maragou V, Shen PK, Tsiakaras P (2009) High surface area tungsten carbide microspheres as effective Pt catalyst support for oxygen reduction reaction. Appl Catal B Environ 89: 223–228

5. Mehta V, Cooper JS (2003) Review and analysis of PEM fuel cell design and manufacturing. J Power Sources 114:32–53

6. Negro E, Noto VD (2008) Polymer electrolyte fuel cells based on bimetallic carbon nitride electrocatalysts. J Power Sources 178: 634–641

7. Costamagna P, Srinivasan S (2001) Quantum jumps in the PEMFC science and technology from the 1960s to the year 2000: Part II. Engineering, technology development and application aspects. J Power Sources 102:253–269

8. Zhang H, Jin MS, Xia YN (2012) Enhancing the catalytic and electrocatalytic properties of Pt-based catalysts by forming bimetallic nanocrystals with Pd. Chem Soc Rev 41:8035–8049

9. Srivastava R, Mani P, Hahn N, Strasser P (2007) Efficient oxygen reduction fuel cell electrocatalysis on voltammetrically dealloyed Pt-Cu-Co nanoparticles. Angew Chem Int Ed 46:8988–8991

10. Li XY, Liu XH, Wang WW, Li L, Lu XQ (2014) High loading Pt nanoparticles on functionalization of carbon nanotubes for fabricating nonenzyme hydrogen peroxide sensor. Biosens Bioelectron 59: 221–226

11. Gasteiger HA, Kocha SS, Sompalli B, Wagner FT (2005) Activity benchmarks and requirements for Pt, Pt-alloy, and non-Pt oxygen reduction catalysts for PEMFCs. Appl Catal B Environ 56:9–35

12. Gasteiger HA, Markovic NM (2009) Just a dream—or future reality? Science 324:48–49

13. Stamenkovic VR, Mun BS, Arenz M, Mayerhofer KJJ, Lucas CA, Wang GF, Ross PN, Markovic NM (2007) Trends in electrocatalysis on extended and nanoscale Pt-bimetallic alloy surfaces. Nat Mater 6:241–247

14. Stamenkovic VR, Fowler B, Mun BS, Wang GF, Ross PN, Lucas CA, Markovic NM (2007) Improved oxygen reduction activity on $Pt_3Ni(111)$ via increased surface site availability. Science 315:493–497

15. Debe MK (2012) Electrocatalyst approaches and challenges for automotive fuel cells. Nature 486:43–51

16. Jung N, Chung DY, Ryu J, Yoo SJ, Sung YE (2014) Pt-based nanoarchitecture and catalyst design for fuel cell applications. Nano Today 9:433–456

17. Suo Y, Zhuang L, Lu JT (2007) First-principles considerations in the design of Pd-alloy catalysts for oxygen reduction. Angew Chem Int Ed 46:2862–2864

18. Liu YQ, Xu C-X (2013) Nanoporous PdTi alloys as non-platinum oxygen reduction reaction electrocatalysts with enhanced activity and durability. Chem Sus Chem 6:78–84

19. Han B, Xu C (2014) Nanoporous PdFe alloy as highly active and durable electrocatalyst for oxygen reduction reaction. Int J Hydrog Energy 39:18247–18255

20. He ZB, Maurice JL, Gohier A, Lee CS, Pribat D, Cojocaru CS (2011) Iron catalysts for the growth of carbon nanofibers: Fe, Fe_3C or both. Chem Mater 23:5379–5387

21. Lu AH, Nitz JJ, Comotti M, Weidenthaler C, Schlichte K, Lehmann CW, Terasaki O, Schüth F (2010) Spatially and size selective synthesis of Fe-based nanoparticles on ordered mesoporous supports as highly active and stable catalysts for ammonia decomposition. J Am Chem Soc 132:14152–14162

22. Mei H, Wu WQ, Yu BB, Wu HM, Wang SF, Xia QH (2016) Nonenzymatic electrochemical sensor based on Fe@Pt core-shell nanoparticles for hydrogen peroxide, glucose and formaldehyde. Sensors Actuators B Chem 223:68–75

23. Nadagouda MN, Varma RS, Greener A (2007) Synthesis of core (Fe, Cu)-shell (Au, Pt, Pd, and Ag) nanocrystals using aqueous vitamin C. Cryst Growth Des 7:2582–2587

24. Kristian N, Yu YL, Lee JM, Liu XW, Wang X (2010) Synthesis and characterization of Co_{core}-Pt_{shell} electrocatalyst prepared by spontaneous replacement reaction for oxygen reduction reaction. Electrochim Acta 56:1000–1007

25. Zhu H, Li XW, Wang FH (2011) Synthesis and characterization of Cu@Pt/C core-shell structured catalysts for proton exchange membrane fuel cell. Int J Hydrog Energy 36:9151–9154

26. Sánchez-Padilla NM, Montemayor SM, Torres LA, Rodríguez Varela FJ (2013) Fast synthesis and electrocatalytic activity of M@Pt (M=Ru, Fe_3O_4, Pd) core-shell nanostructures for the oxidation of ethanol and methanol. Int J Hydrog Energy 38:12681–12688

27. Teng XW, Black D, Watkins NJ, Gao YL, Yang H (2003) Platinum-maghemite Core-shell nanoparticles using a sequential synthesis. Nano Lett 3:261–264

28. Sarkar A, Manthiram A (2010) Synthesis of Pt@Cu core-shell nanoparticles by galvanic displacement of Cu by Pt^{4+} ions and their application as electrocatalysts for oxygen reduction reaction in fuel cells. J Phys Chem C 114:4725–4732

29. Mei H, Wu HM, Wu WQ, Wang SF, Xia QH (2015) Ultrasensitive electrochemical assay of hydrogen peroxide and glucose based on PtNi alloy decorated MWCNTs. RSC Adv 5:102877–102884

30. Mei H, Wu WQ, Yu BB, Wu HM, Wang SF, Zhang XH, Xia QH (2016) Electrochemical sensor for detection of glucose based on Ni@Pt core-shell nanoparticles supported on carbon. Electroanalysis 28:671–678

31. Wu BH, Hu D, Kuang YJ, Liu B, Zhang XH, Chen JH (2009) Functionalization of carbon nanotubes by an ionic-liquid polymer: dispersion of Pt and PtRu nanoparticles on carbon nanotubes and their electrocatalytic oxidation of methanol. Angew Chem Int Ed 48:4751–4754

32. Lu J, Bo X, Wang H, Guo L (2013) Nitrogen-doped ordered mesoporous carbons synthesized from honey as metal-free catalyst for oxygen reduction reaction. Electrochim Acta 108:10–16

33. Mayrhofer KJJ, Strmcnik D, Blizanac BB, Stamenkovic V, Arenz M, Markovic NM (2008) Measurement of oxygen reduction activities via the rotating disc electrode method: from Pt model surfaces to carbon-supported high surface area catalysts. Electrochim Acta 53:3181–3188

34. Dai L, Xue Y, Qu L, Choi HJ, Baek JB (2015) Metal-free catalysts for oxygen reduction reaction. Chem Rev 115:4823–4892

35. Zheng Y, Jiao Y, Jaroniec M, Jin Y, Qiao SZ (2012) Nanostructured metal-free electrochemical catalysts for highly efficient oxygen reduction. Small 8:3550–3566

36. Shao M, Chang Q, Dodelet JP, Chenitz R (2016) Recent advances in electrocatalysts for oxygen reduction reaction. Chem Rev 116: 3594–3657

37. Higgins D, Zamani P, Yu A, Chen Z (2016) The application of graphene and its composites in oxygen reduction electrocatalysis: a perspective and review of recent progress. Energy Environ Sci 9: 357–390

38. Favaro M, Ferrighi L, Fazio G, Colazzo L, Valentin CD, Durante C, Sedona F, Gennaro A, Agnoli S, Granozzi G (2015) Single and multiple doping in graphene quantum dots: unraveling the origin of selectivity in the oxygen reduction reaction. ACS Catal 5:129–144